Directional Emission from Leaky and Guided Modes in GaAs Nanowires Measured by Cathodoluminescence

Benjamin J. M. Brenny,[†] Diego R. Abujetas,[‡] Dick van Dam,[¶] José A. Sánchez-Gil,[‡] J. Gómez Rivas,[¶,§] and Albert Polman[*,†]

[†]*Center for Nanophotonics, FOM Institute AMOLF, Science Park 104, 1098 XG Amsterdam, The Netherlands*

[‡]*Instituto de Estructura de la Materia (IEM-CSIC), Consejo Superior de Investigaciones Científicas, Serrano 121, 28006, Madrid, Spain*

[¶]*COBRA Research Institute, Eindhoven University of Technology, P.O. Box 513, 5600 MB Eindhoven, The Netherlands*

[§]*FOM Institute DIFFER, P.O. Box 6336, 5600 HH Eindhoven, The Netherlands*

E-mail: polman@amolf.nl

Abstract

We measure the polarization-resolved angular emission distribution from thin (diameter ∼110 nm) and thick (diameter ∼180 nm) GaAs nanowires with cathodoluminescence polarimetry. The nanowires, which are horizontally resting on a thin carbon film, are excited by a 5 keV electron beam and emit bandgap luminescence at a central wavelength of 870 nm. The emission can couple to different waveguide modes that propagate along the wire. These waveguide modes are dependent on the wire diameter and determine the directionality and polarization of the emission. Although each measured nanowire can support different modes, the polarized emission is dominated by the

TM01 waveguide mode in all cases, independently of wire diameter. When exciting the nanowires away from the center, close to the end facets, the thin and thick wires exhibit an opposite directional emission. The emission from thin nanowires is dominated by a leaky TM01 mode that leads to emission in the opposite direction to the excitation position. For the thick wires, however, the TM01 mode is guided but also lossy due to absorption in the substrate. In that case, the wires emit towards the same direction as the excitation position. We show that the measurements agree well with both a simple 1D current model and numerical simulations. The high spatial resolution of angular and polarization resolved cathodoluminescence spectroscopy provides detailed insight into the nanoscale emission and propagation of light in semiconductor nanowires.

Keywords

Cathodoluminescence, nanowires, GaAs, polarimetry, waveguide modes

Semiconductor nanowires have fueled a growing field of integrated nanoscale optoelectronic devices, such as lasers,[1–3] light emitting diodes,[4–6] photovoltaics,[7–10] single-photon detectors,[11–14] photodetectors[15] and metamaterials.[16,17] Both the electrical and optical properties of nanowires are eminently tunable by controlling their size, geometry or composition, among others.[18–21] The directionality and polarization of emitted radiation from nanowires have been examined in previous studies[15,22–24] and result from the coupling to leaky and guided waveguide modes,[25–30] which can also be described by Mie and Fabry-Pérot resonances.[30,31] All modes are highly dependent on nanowire diameter.

Most previous studies of semiconductor nanowire emission properties have employed optical excitation methods. While powerful, such techniques lack the nanoscale spatial resolution to uncover all the features of the radiative processes from these nanostructures. Here we use cathodoluminescence (CL) spectroscopy, in which an electron beam acts as a highly localized excitation source and the emitted light is detected.[32–34] The high spatial excitation resolution of CL is typically determined by the electron beam spot size and the evanescent

field extent about the beam path (∼10–30 nm),[34] which enables the study of the nanoscale modal behavior of light.[35–38] In general, CL also allows the characterization of a wide range of material properties.[39–42] Recently, the ability to measure both the angular and polarization distribution in CL has been demonstrated.[43,44]

In this article, we use these new CL features to investigate the angle- and polarization-dependent emission from horizontal GaAs nanowires.[43] We study nanowires of different lengths and diameters that support both leaky and guided modes. Exciting the nanowires along their length, we find that the TM01 mode dominates the polarization-resolved emission for all excited wires, but depending on the diameter, the mode is either leaky or guided. We observe a distinct change of the directionality of the CL emission when exciting the nanowires close to their end facets, which correlates with the nanowire diameter and the nature of the mode. Thinner, leaky wires emit in the opposite direction from thicker, guided wires. The measurements show good agreement with both a simple 1D current model and numerical simulations, which show that the substrate also plays a role in the emission directionality.

Experiment

GaAs nanowires were grown by self-catalyzed molecular beam epitaxy on silicon[45,46] and were subsequently mechanically broken and deposited on a holey carbon TEM grid (see also Methods). Scanning electron micrographs of the two GaAs nanowires studied here are shown in Figure 1(a). The thin NW1 has a length of 7.9 μm and a diameter of 100–120 nm, while the thick NW2 has a length of 12 μm and a diameter of 175–195 nm (both are slightly tapered). Both nanowires are lying horizontally on the ∼20 nm thick carbon layer. In the Supporting Information we show data for an additional thin and thick wire (SEM images shown in Figure S1).

The cathodoluminescence spectroscopy and polarimetry setup[43,47,48] is schematically shown in Figure 1(b). The radiation from the nanowires is collected by a parabolic mir-

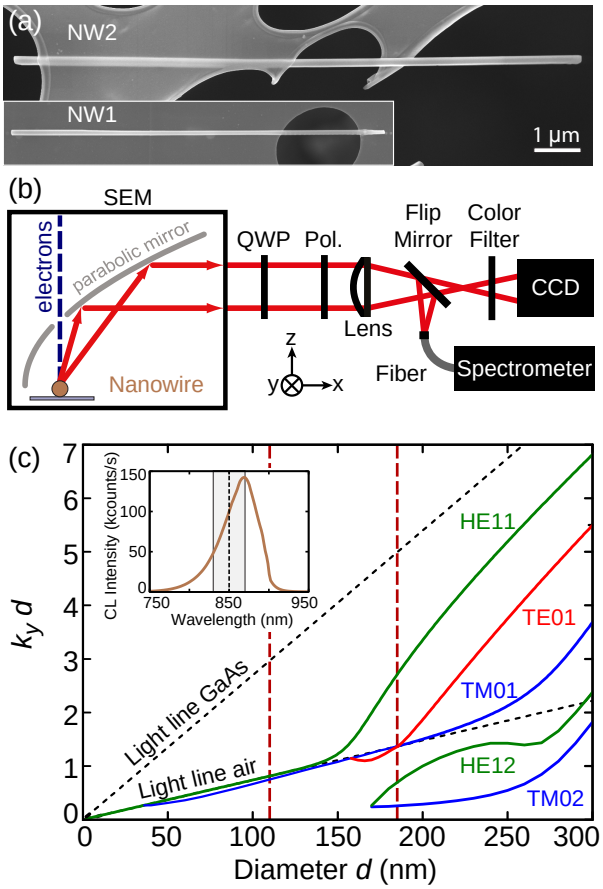

Figure 1: (a) Scanning electron micrographs of the GaAs nanowires NW1 (bottom) and NW2 (top), shown on the same scale. NW1 is 7.9 µm long and 100–120 nm thick; NW2 is 12 µm long and 175–195 nm thick. (b) Schematic overview of the cathodoluminescence polarimetry setup. The electron beam excites the nanowires, the emitted radiation is collected by a parabolic mirror and either focused onto a fiber connected to a spectrometer or sent through a QWP, linear polarizer and bandpass filter before being imaged onto a 2D CCD camera. (c) Dispersion relation of leaky and guided modes for infinitely long cylinders, showing the real part of the wavevector k_y multiplied by the cylinder diameter d, as a function of d, for GaAs at $\lambda_0 = 850$ nm ($n = 3.6$, $k_0 = 7.39$ µm^{-1}). The vertical red dashed lines indicate the average diameters of the two wires. The inset shows the measured CL emission spectrum from NW2. The spectrum of NW1 (not shown) does not differ noticeably except for a lower intensity. The vertical black dashed line in the inset at $\lambda_0 = 850$ nm indicates the transmittance maximum of the bandpass filter used for the angular measurements, while the gray area indicates the 40 nm bandwidth of the filter.

ror and directed onto a spectrometer or filtered by a bandpass filter and imaged onto a 2D camera to measure the angular intensity distribution for a given wavelength. Polarization-resolved measurements are obtained by using a polarimeter composed of a quarter-wave

plate (QWP) and a linear polarizer (Pol.), with which the Stokes parameters of the emitted radiation and therefore the different electric field components can be determined.[49] We correct for the geometrical and polarization dependent transformations of the parabolic mirror on the measured emission[43] (see Methods for more details about the CL measurements). For the measurements, the nanowires are aligned along the y-axis, as defined by the coordinate system shown in Figure 1(b). As we expect directional emission along the nanowire axis, this is the preferred orientation to have symmetric collection by the mirror. The CL emission spectrum from NW2 is shown in the inset of Figure 1(c) and is dominated by band-gap recombination centered around $\lambda_0 = 870$ nm. This emission can feed into waveguide modes supported by the nanowire, that depend on its diameter, and which can affect the polarization and directionality of the emitted radiation.[23–25,29]

Nanowire waveguide modes

Figure 1(c) shows the dispersion of waveguide modes for infinitely long cylinders,[50] calculated for GaAs at $\lambda_0 = 850$ nm ($n = 3.6$, $k_0 = 7.39$ μm^{-1}), the wavelength at which we filter the angle-resolved measurements. We follow the formalism used in Ref. 28 and determine the wavevector k_y along the axis of the nanowire. We show the real part of k_y multiplied by the wire diameter d, as a function of d. The dispersion curves denote transverse electric (TE), transverse magnetic (TM), and magnetoelectric (HE) modes. These modes are characterized as "leaky" if their dispersion lies below the light line of air ($k_y < k_0$), in which case they also posses a non-negligible imaginary part of the wavevector k_y.[28] If the mode dispersion lies above the light line of air but below the light line in GaAs ($k_{GaAs} > k_y > k_0$), the waveguide mode is guided within the nanowire.

The vertical red dashed lines in Figure 1(c) display the average diameter of the two nanowires studied here. For the thin NW1 (and any nanowire with a diameter below 150 nm), only the TM01 and the HE11 modes are supported. Both are very close to the light

line in air, but the TM01 mode is slightly below it and thus leaky for these diameters. In the case of the thicker NW2, the TE01, HE12 and TM02 also occur. The latter two are far below the light line in air and thus have a very short propagation length along the nanowire, while the HE11 mode is very clearly guided. The TE01 and TM01 modes are both very close to the light line of air in this region, representing a transition region between a leaky and guided nature for these modes. Which modes will dominate the emission depends on the coupling efficiency between the excitation source and the mode.

The dispersion relation allows us to determine which modes can play a role in the emission from these nanowires and to calculate the wavevector corresponding to each mode for a given diameter. A 1D current model, developed in Ref. 28 and applied in Ref. 24, uses the wavevectors to calculate far field emission patterns for all electromagnetic field components. The model describes the nanowire as a 1D cavity in vacuum with length L; the emission is produced by a line current excited by a dipole at a given position along the wire. This simple model allows us to retrieve the expected polarization-dependent angular emission patterns for different modes at different wire diameters, which we can compare to measurements.

CL polarimetry

We measure and calculate the angle- and polarization-dependent emission intensity distributions at $\lambda_0 = 850$ nm for central excitation of the two nanowires and clearly recognize the TM01 mode as being the dominant contribution, as shown in Figure 2. For NW1 we compare the measurements (Figures 2(a–c)) to the 1D calculation for the TM01 mode (Figures 2(d–f)), displaying the Cartesian electric field intensities $|\mathrm{E}_x|^2$, $|\mathrm{E}_y|^2$ and $|\mathrm{E}_z|^2$ as a function of azimuthal (φ) and zenithal (θ) angles. The field orientations are indicated by the coordinate system at the left, and the wires are oriented along the y axis. A wavevector of $k_y = 6.63 + i\ 1.19\ \mu\mathrm{m}^{-1}$ was used for the calculation, as determined from the dispersion relation and nanowire diameter. The dark blue regions around the edges of each image

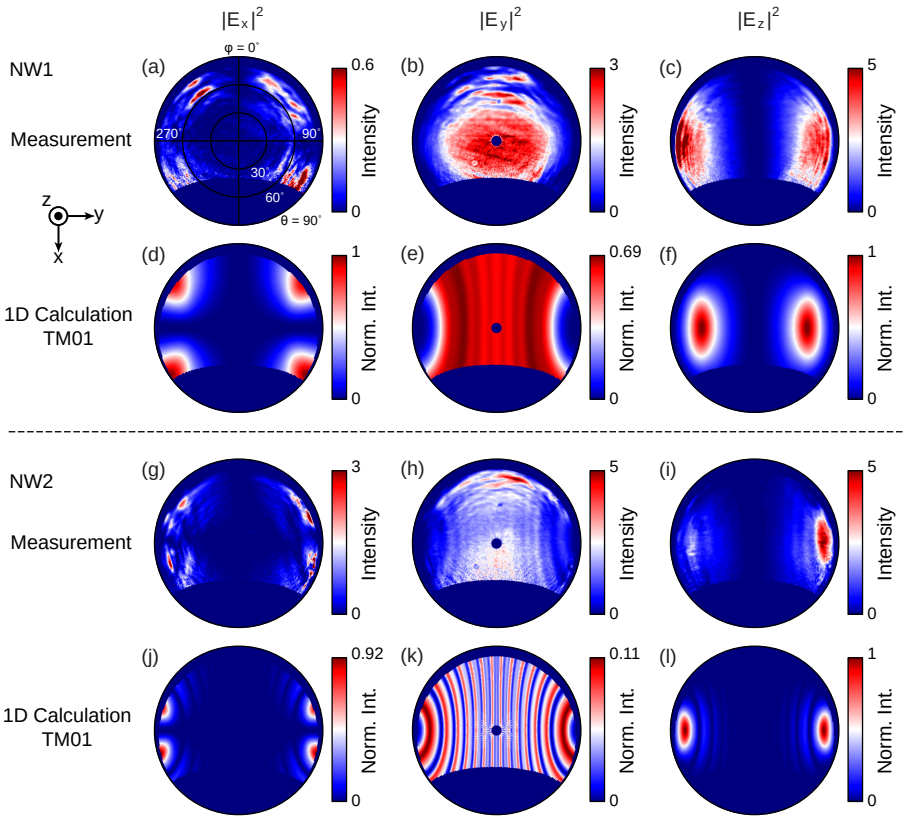

Figure 2: Measured (a-c, g-i) and calculated (d-f, j-l) angular emission distributions of the Cartesian field intensities at $\lambda_0 = 850$ nm for NW1 (a-f) and NW2 (g-l), as a function of azimuthal (φ) and zenithal (θ) angles. The patterns were measured and calculated for central excitation of the nanowires. (a, d, g, j) show the intensity of the E_x field component, (b, e, h, k) the intensity of E_y, and (c, f, i, l) the intensity of E_z (the coordinate system is shown in the top left). The calculations for each wire have been normalized to their maximum. The measured intensities are given in 10^6 counts sr^{-1} s^{-1}.

correspond to the angles at which no light is collected by the mirror. The intensity scale is chosen so as to maximize the contrast in the color scale to better view the details of the features. In the case of the calculation the intensities are normalized to the overall maximum value for each wire. We observe excellent qualitative agreement between measurement and calculation. For $|E_x|^2$ (Figures 2(a,d)) there are four bright features at large zenithal angles, while $|E_y|^2$ (Figures 2(b,e)) displays bright emission in the center of the mirror and $|E_z|^2$ (Figures 2(c,f)) exhibits two lobes to the left and right of the polar image, in the directions of the end facets of the nanowire.

For NW2 too we observe very similar features for both measurements (Figures 2(g–i))and calculations (Figures 2(j–l)). A wavevector of $k_y = 8.00 + i\ 0.50\ \mu m^{-1}$ was used for the calculation. For $|E_x|^2$ (Figures 2(g,j)) we observe four features at even higher zenithal angles than for NW1, at the corners of the angular range. $|E_y|^2$ (Figures 2(h,k)) shows the brightest intensity in the center, as for NW1, but this time we can also see intensity fringes along the vertical direction, which are due to interference between the emission from the nanowire end facets. The fringes are clearly visible in the experiment, but with lower contrast than in the calculations, which we attribute to imperfections in the mirror and the nanowire end facets, and to limitations on the angular resolution. Finally, $|E_z|^2$ (Figures 2(i,l)) again displays two lobes to the left and right, but at higher angles than for NW1, similarly to the behavior of $|E_x|^2$. In the experiment, the two lobes are asymmetric, which we attribute to the slight tapering of the wire.

Comparing the relative intensities of calculations and measurements for both nanowires, we find that $|E_x|^2$ is weaker and $|E_y|^2$ is stronger in the measurements than in the calculations. We ascribe this discrepancy to a lower collection efficiency at the edges of the mirror where the $|E_x|^2$ component is strongest, while the $|E_y|^2$ component is brightest in the central regions of the mirror and thus does not suffer from this problem.

Even though the two nanowires have quite different diameters, in both cases we can clearly recognize very similar polarized field distributions that show excellent qualitative agreement with calculations for the TM01 mode. From this we conclude that the emission behavior of both NW1 and NW2 is dominated by the TM01 mode. Differences between the two wires are expected, however, because for NW1 the mode is leaky ($Re(k_y) = 6.6 < k_0 = 7.39\ \mu m^{-1}$), while for NW2 it is guided ($Re(k_y) = 8.00 > k_0 = 7.39\ \mu m^{-1}$). To support the data, we show polarization-resolved measurements for an additional thin and thick nanowire in Figure S2 of the Supporting Information, which exhibit the same type of features for all three field components as the results shown here.

Directional emission

Next, we study the directional behavior of the nanowire emission for excitation off-center, near the end facets of the wires, observing a distinct difference in the directionality of the emission between NW1 and NW2, as shown in Figure 3. We compare the total intensity emitted by both wires as a function of the azimuthal and zenithal angles in the case of measurements, calculations and simulations, for excitation at the left edge, center, and right edge. The edge excitation is always a few hundred nm away from the end facet, with the exact positions shown by the dashed lines in Figure 4. The measured intensities differ between the wires and excitation positions, which we attribute to variations in local material quality and size of the interaction volume (due to tapering and different diameters). For the measurements on NW1, central excitation (Figure 3(b)) results in two symmetric lobes of higher intensity to the left and right, while excitation at the left edge (Figure 3(a)) leads to directional emission to the right side and excitation on the right (Figure 3(c)) leads to emission towards the left side. 1D calculations of the total emission intensity from the leaky TM01 mode qualitatively reproduce the emission behavior for excitation in the center and 300 nm from the end facets (Figures 3(d–f)). In the measurements, the electron beam excitation at the edges was ∼300–500 nm from the end facets.

We attribute the discrepancies between experiment and calculations in the shape of the emission patterns to the fact that the excitation volume can be much larger than the electron beam width (up to a few hundred nm). This is due to electron scattering, secondary electron generation, carrier diffusion, and photon recycling, which can play a large role in such a direct band gap material.[44,51,52] A large majority of the excitations will occur very close to the point of impact, but light generation will nevertheless cover a larger area, while the calculations assume a point-source excitation. The presence of the thin holey carbon substrate, which is not taken into account in the calculation, can also affect the emission, as we will now show for NW2.

The measurements on the thicker NW2 (Figures 3(g–i)) show the opposite directionality

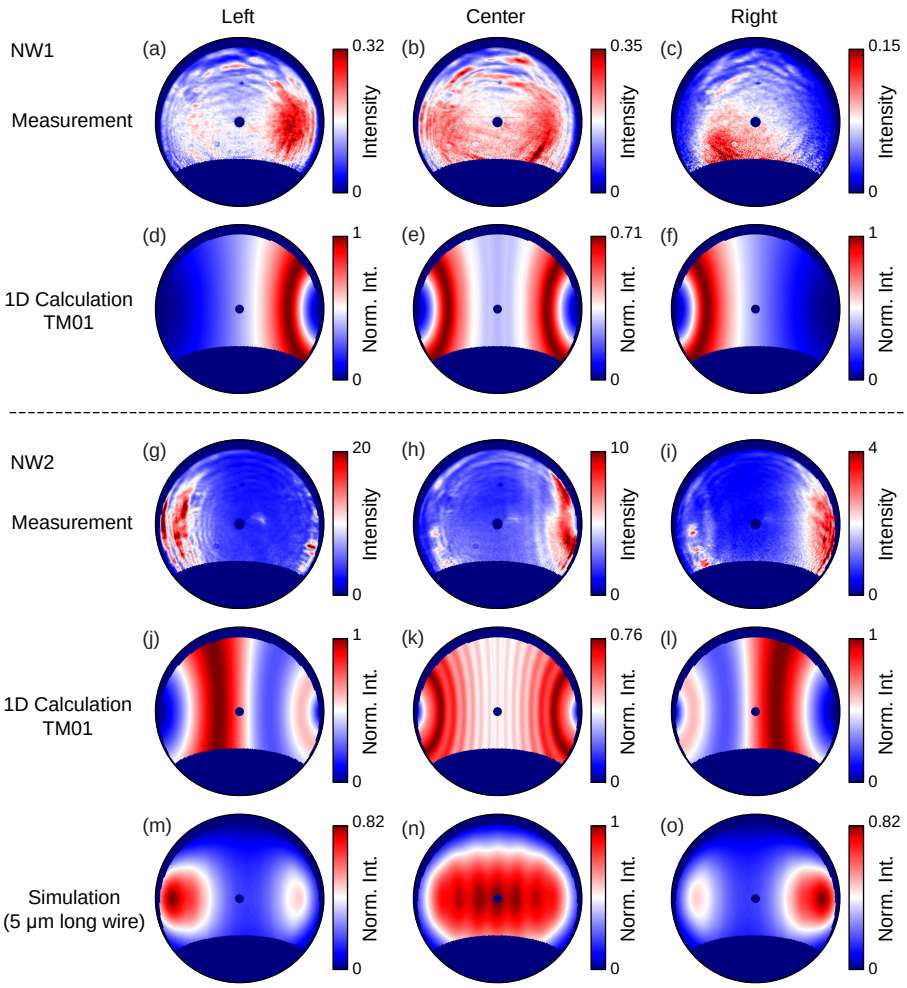

Figure 3: Measured (a-c, g-i), calculated (d-f, j-l) and simulated (m-o) angular emission distributions of the total intensity at $\lambda_0 = 850$ nm for NW1 (a-f) and NW2 (g-o). The patterns were measured and calculated for excitation at the left (a, d, g, j, m), center (b, e, h, k, n) and right (c, f, i, l, o) of the nanowires (see Figure 4 for positions). The calculations and simulations for each wire have been normalized to their maximum. The measured intensities are given in 10^6 counts sr^{-1} s^{-1}. The 1D calculation uses the same wire lengths as in the experiment (7.9 and 12 µm), but due to computational constraints the simulated NW2 is shorter (5 µm).

to that of NW1. Excitation at the left edge leads to emission towards the left, while excitation at the right edge produces emission towards the right. The excitation positions were 700 nm (left) and 400 nm (right) away from the end facets (see also the dashed lines in Figure 4(b)). For central excitation we observe asymmetrical emission, as was the case for Figure 2(i), which we again attribute to the tapering of the wire that creates an inherent asymmetry

in the wire and its emission properties. The leaky mode in the thin wire is less affected by tapering as radiation is emitted continuously as the mode propagates along the wire. The thicker NW2 on the other hand, supports a guided mode, so light has a much longer propagation length, traveling through the wire for multiple round-trips. Since the modal properties are very sensitive to the diameter, more light will be affected by the gradual variations in modal behavior along the length of the wire.

We first compare the measurements to the 1D calculations of the (guided) TM01 mode, which do not directly take into account the substrate (Figures 3(j–l)). We represent absorption at the band edge and losses into the substrate by an imaginary part of k_y of 0.50 i μm^{-1}. We find for excitation near the edges (500 nm away from the end facet, similarly to the measurement) a maximum in emission to the same side as in the measurements, with a weaker feature in the opposite direction. We note that also in the measurements of NW2 there is a region of higher intensity to the opposite side of the dominant emission. For central excitation, we observe quite good qualitative agreement between experiment and calculation, taking into account the asymmetry we attribute to tapering of the wire. For this long wire, interference fringes from the emission of both facets are expected, as shown in Figure 3(k), which are also faintly visible in Figure 3(h).

To get a better measure for the effect of the substrate, we perform numerical simulations using COMSOL (see Methods for more details) on a 180 nm thick and 5 μm long wire on a semi-infinite carbon substrate (Figures 3(m–o)). Due to computational constraints we did not simulate a 12 μm long wire nor the extremely thin substrate The simulations, however, do show good qualitative agreement with the experiment and provide insight into the role of the substrate on the emission behavior. Central excitation leads to a symmetric emission profile with highest intensity in the central region and interference fringes that are less distinct than for the 1D calculation. Excitation at the edges (500 nm from the end facet) shows emission profiles in good qualitative agreement with the measurements, with a bright feature to the same side at high angles and a weaker spot on the opposite side. Both

the 1D calculations and the simulations predict the measured directionality. The features measured for edge excitation closely resemble the simulation, while there is better agreement with the 1D calculation for central excitation. As the substrate is very thin, we can expect it to have a smaller effect than in the simulation that was performed for a semi-infinite substrate. Indeed, a combination of the 1D calculations and simulations would reproduce the measured data better, but in each case there is a clear directional emission towards the same side as the excitation position, completely opposite to the behavior of NW1. The importance of the substrate as an additional loss channel does not play a large role in the case of the leaky mode ($k_y < k_0$) as there is already a strong inherent leakage. For the thicker wire, simulations without substrate show an emission directionality that is more strongly dependent on excitation position and near the edges becomes opposite to that observed in the measurements (Figure S4 and Figure S5 in the Supporting Information). We conclude that both the guided behavior of the TM01 mode and the additional loss channel due to the substrate play a role in determining the directional emission behavior of the thick nanowire.

We can study the directional behavior of the emission as a function of the excitation position more closely taking advantage of the high spatial resolution of the electron beam. Figure 4 shows the emission directionality for both wires when scanning the beam along their length. We determine a left-to-right ratio L-R/L+R by averaging the total intensity over all zenithal angles in 60° azimuthal wedges on the left and right sides, as these correspond to the regions of highest intensity features. The gray bands correspond to positions that are outside the wires and the dashed lines indicate the positions of the measurements in Figure 3. Comparing NW1 (Figure 4(a)) to NW2 (Figure 4(b)), we observe that there is no left/right directionality at the very edges for both wires, but that close to the edges the left-to-right ratio is reversed for the two wires, as described above. The directionality of NW2 is more asymmetric, which we attribute to the tapering that affects the guided wave in a stronger fashion than for the leaky case. Figure S3 in the Supporting Information shows the left-to-right ratio for the additional thin and thick wires discussed previously, which display

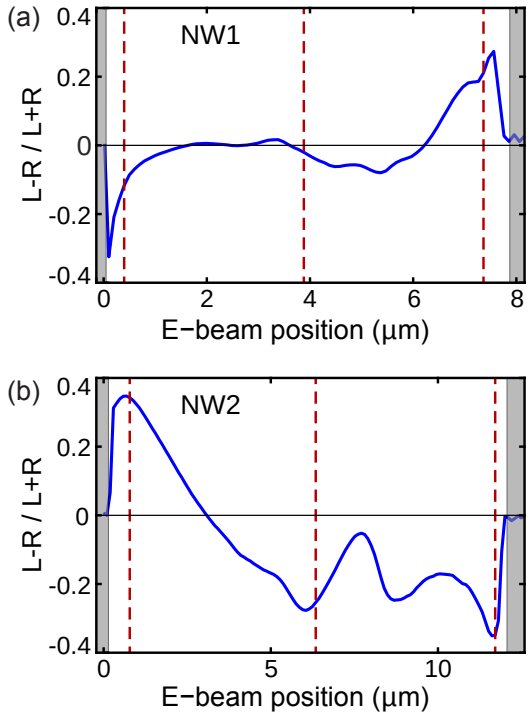

Figure 4: Ratio of the left-to-right directional emission for NW1 (a) and NW2 (b), showing the ratio (L-R)/(L+R) as a function of the electron beam position as it scans along the wire. The gray bands indicate positions that are not on the wire, while the red dashed lines indicate the positions of the left, center and right measurements shown in Figure 3. The leftwards and rightwards directional intensities were determined by averaging the total intensity over all zenithal angles in 60° azimuthal wedges (φ=240–300° for left and φ=60–120° for right).

the same behavior as the wires shown here. Figure S5 in the Supporting Information shows the left-to-right ratio for simulations of a thick wire with and without substrate, showing agreement between the measurements for thick wires and the simulation with substrate.

Conclusion

In conclusion, we have demonstrated that cathodoluminescence emission from GaAs nanowires is strongly directional and depends on the nanowire diameter. The emission excited by the electron beam couples to waveguide modes that determine the polarization and angular distribution of the outcoupled radiation. These waveguide modes are very sensitive to wire diameter, especially when they change in nature from leaky to guided when crossing the light

line in air. Polarization-resolved measurements show that the emission from both nanowires studied here is dominated by a TM01 mode. The leaky TM01 mode supported by the thin wire displays emission in the direction opposite from the excitation position, while the thick wire supporting the guided TM01 mode exhibits emission in the same direction. Both the leaky/guided nature of mode and the presence of the substrate play an important role in determining the emission directionality. Cathodoluminescence polarimetry proves to be a powerful technique to study the angular- and polarization-dependent emission properties of semiconducting nanowires or other nanostructures, with a subwavelength excitation resolution.

Methods

Sample fabrication

The GaAs nanowires were grown on Si(111) undoped wafer via a Ga-assisted method in a DCA P600 solid-source MBE machine.[45,46] Typical growth parameters are as follows: a Ga rate of 0.3 Å/s as flux of 2.5×10^{-6} torr, a substrate temperature of 640 °C, rotation of the substrate at 7 r.p.m., and a V/III beam equivalent pressure ratio of 50. The nanowires were removed from the silicon substrate in an isopropanol solution by ultrasonic bath for 1 minute. A few drops of the isopropanol solution containing nanowires were transferred to a holey carbon TEM grid (Plano GmbH).

CL measurements

The measurements were performed in a FEI XL-30 SFEG (5 keV electron beam, ∼0.1 nA current) equipped with a home-built CL system.[34,47,48] The emission excited by the electron beam is collected by an aluminium paraboloid mirror and directed to an optical setup. We measure either the spectrum using a liquid-nitrogen-cooled back-illuminated silicon CCD array (Princeton Instruments Spec-10 100B), or the angular emission profile using a Peltier-

cooled back-illuminated 2D silicon CCD array (Princeton Instruments PIXIS 1024B).[47,48] To determine the full emission polarization, we use a series of six measurements of the angular CL distribution using the 2D CCD array in conjunction with a quarter-wave plate (QWP) and linear polarizer (LP). Each measurement was taken for a different combination of QWP and LP settings (horizontal, vertical, 45°, 135°, right- and left-handed circular). We correct for the geometrical and polarization dependent response of the paraboloid mirror on the CL emission it redirects to the optical setup.[43] A 40 nm bandpass color filter was used to spectrally select the measured emission at $\lambda_0 = 850$ nm. Integration times of 0.1–1 s were used depending on sample brightness. For every setting of the QWP and LP, we collected a dark reference measurement where we blank the electron beam (using the same integration time as for the corresponding CL measurement). This reference was subtracted from the data in the post-processing stage. Possible sources of errors on the measurements include drift of the electron beam, bleaching/contamination during measurements which leads to a reduction in CL signal, and fluctuations in the current and/or the alignment of the mirror.

FEM simulations

The finite-element-method (FEM) simulations of the far field emission profiles of finite nanowires were performed using the commercial sofware package COMSOL Multiphysics v4.3b, using the same methods as in Ref. 28 and Ref. 24. For free-standing nanowires the simulation space consisted of a circular cylinder of length L and diameter d that represents the nanowire, enclosed in three concentric spheres of diameter $L+2\lambda_0$, $L+4\lambda_0$, and $L+6\lambda_0$, with their centers coinciding with that of the cylinder. The innermost two spheres were set to be air (n_{air}), while the outermost layer was defined as a perfectly matched layer (PML) to absorb all outgoing radiation and prevent reflections. The material constants of GaAs for the cylinder were taken from Palik[53] ($n_{GaAs} = 3.6$ at $\lambda_0 = 850$ nm). A tetrahedral mesh was used, with maximum elements sizes (MES) of 25 nm in the domain of the cylinder and 160 nm for the air domains. The maximum element growth rate was set to 1.35 for all of the

domains

For nanowires on top of a carbon substrate the geometry is modified as follows. The three concentric spheres of the same diameter are divided into two semi-spherical layered domains through a plane that contains the cylinder axis and the cylinder is then shifted by $d/2$ from its original position in order to be placed on top of one of the new semi-spherical spaces, which we refer to as the substrate. The substrate was set to be amorphous carbon ($n_C = 1.987 + i\ 0.83$ at $\lambda_0 = 850$ nm)[54] and the rest was set to be air, except for the GaAs cylinder. As the space was divided into two different media, the material properties of the outermost PML must be the same as the adjacent medium. The MES of the tetrahedral mesh was 25 nm for the cylinder, 160 nm for the air and 90 nm for the substrate. The maximum element growth rate was 1.35, the same as for the free-standing nanowires.

Simulations were highly memory-demanding; in the case of the nanowires of length $L = 5$ μm on top of the substrate, the calculations need ∼400 GB. Post-processing calculations were used to determine the total radiated power at the inner spherical boundary $\sum_{int}$, defined by:

$$P = \int_{\sum_{int}} \langle \mathbf{S} \rangle \cdot \mathbf{n} dS \tag{1}$$

where $\mathbf{n}$ is the outward normal unit-vector to the surface.

Supporting Information Available

The Supporting Information contains additional data from another two measured nanowires, as well as simulations that compare the emission behavior with and without the substrate.

This material is available free of charge via the Internet at `http://pubs.acs.org/`.

Author Information

Corresponding Authors

*E-mail (A. Polman): polman@amolf.nl.

Notes

A.P. is co-founder and co-owner of Delmic BV, a startup company developing a commercial product based on the cathodoluminescence system that was used in this work.

Acknowledgement

The authors acknowledge Clara Osorio, Mark Knight and Toon Coenen for fruitful discussions. We also thank Mohammad Ramezani, G. Tütüncüoglu, F. Matteini, and A. Fontcuberta i Morral for providing the GaAs sample. This work is part of the "Stichting voor Fundamenteel Onderzoek der Materie (FOM)" as well as the Dutch technology foundation STW, which are financially supported by the "Nederlandse Organisatie voor Wetenschappelijk Onderzoek (NWO)" and the Dutch Ministry of Economic Affairs. It is also part of NanoNextNL, a nanotechnology program funded by the Dutch Ministry of Economic Affairs, part of an industrial partnership program between Philips and FOM, and is supported by the European Research Council (ERC). The Spanish "Ministerio de Economía y Competitividad" is also acknowledged for financial support through the grants NANOPLAS+ (FIS2012-31070) and LENSBEAM (FIS2015-69295-C3-2-P).

References

(1) Huang, M. H.; Mao, S.; Feick, H.; Yan, H.; Wu, Y.; Kind, H.; Weber, E.; Russo, R.; Yang, P. Room-temperature ultraviolet nanowire nanolasers. *Science* **2001**, *292*, 1897–

1899.

(2) Vanmaekelbergh, D.; van Vugt, L. K. ZnO nanowire lasers. *Nanoscale* **2011**, *3*, 2783–2800.

(3) Röder, R.; Ploss, D.; Kriesch, A.; Buschlinger, R.; Geburt, S.; Peschel, U.; Ronning, C. Polarization features of optically pumped CdS nanowire lasers. *J. Phys. D: Appl. Phys.* **2014**, *47*, 394012.

(4) Haraguchi, K.; Katsuyama, T.; Hiruma, K. Polarization dependence of light emitted from GaAs p-n junctions in quantum wire crystals. *J. Appl. Phys.* **1994**, *75*, 4220–4225.

(5) Svensson, C. P. T.; Mårtensson, T.; Trägårdh, J.; Larsson, C.; Rask, M.; Hessman, D.; Samuelson, L.; Ohlsson, J. Monolithic GaAs/InGaP nanowire light emitting diodes on silicon. *Nanotechnology* **2008**, *19*, 305201.

(6) Wierer, J. J.; David, A.; Megens, M. M. III-nitride photonic-crystal light-emitting diodes with high extraction efficiency. *Nat. Photonics* **2009**, *3*, 163–169.

(7) Wallentin, J.; Anttu, N.; Asoli, D.; Huffman, M.; Åberg, I.; Magnusson, M. H.; Siefer, G.; Fuss-Kailuweit, P.; Dimroth, F.; Witzigmann, B.; Xu, H. Q.; Samuelson, L.; Deppert, K.; Borgström, M. T. InP Nanowire Array Solar Cell Achieving 13.8% Efficiency by Exceeding the Ray Optics Limit. *Science* **2013**, *339*, 1057–1060.

(8) Cui, Y.; Wang, J.; Plissard, S. R.; Cavalli, A.; Vu, T. T. T.; van Veldhoven, R. P. J.; Gao, L.; Trainor, M.; Verheijen, M. A.; Haverkort, J. E. M.; Bakkers, E. P. A. M. Efficiency enhancement of InP nanowire solar cells by surface cleaning. *Nano Lett.* **2013**, *13*, 4113–7.

(9) Krogstrup, P.; Jørgensen, H. I.; Heiss, M.; Demichel, O.; Holm, J. V.; Aagesen, M.; Nygard, J.; Fontcuberta i Morral, A. Single-nanowire solar cells beyond the Shockley-Queisser limit. *Nat. Photonics* **2013**, *7*, 306–310.

(10) Muskens, O. L.; Gómez Rivas, J.; Algra, R. E.; Bakkers, E. P. A. M.; Lagendijk, A. Design of light scattering in nanowire materials for photovoltaic applications. *Nano letters* **2008**, *8*, 2638–2642.

(11) Claudon, J.; Bleuse, J.; Malik, N. S.; Bazin, M.; Jaffrennou, P.; Gregersen, N.; Sauvan, C.; Lalanne, P.; Gérard, J.-M. A highly efficient single-photon source based on a quantum dot in a photonic nanowire. *Nat. Photonics* **2010**, *4*, 174–177.

(12) Heiss, M. et al. Self-assembled quantum dots in a nanowire system for quantum photonics. *Nat. Mater.* **2013**, *12*, 439–444.

(13) Bulgarini, G.; Reimer, M. E.; Bouwes Bavinck, M.; Jöns, K. D.; Dalacu, D.; Poole, P. J.; Bakkers, E. P. A. M.; Zwiller, V. Nanowire Waveguides Launching Single Photons in a Gaussian Mode for Ideal Fiber Coupling. *Nano Lett.* **2014**,

(14) Reimer, M. E.; Bulgarini, G.; Akopian, N.; Hocevar, M.; Bavinck, M. B.; Verheijen, M. A.; Bakkers, E. P. A. M.; Kouwenhoven, L. P.; Zwiller, V. Bright single-photon sources in bottom-up tailored nanowires. *Nature communications* **2012**, *3*, 737.

(15) Wang, J.; Gudiksen, M. S.; Duan, X.; Cui, Y.; Lieber, C. M. *Science* **2001**, *293*, 1455.

(16) Paniagua-Domínguez, R.; Abujetas, D. R.; Sánchez-Gil, J. A. Ultra low-loss, isotropic optical negative-index metamaterial based on hybrid metal-semiconductor nanowires. *Sci. Rep.* **2013**, *3*, 1507.

(17) Ramezani, M.; Casadei, A.; Grzela, G.; Matteini, F.; Tütüncüoglu, G.; Rüffer, D.; Fontcuberta i Morral, A.; Gómez-Rivas, J. Hybrid semiconductor nanowire-metallic Yagi-Uda antennas. *Nano Lett.* **2015**,

(18) Yan, R.; Gargas, D.; Yang, P. Nanowire photonics. *Nat. Photonics* **2009**, *3*, 569–576.

(19) Duan, X.; Huang, Y.; Cui, Y.; Wang, J.; Lieber, C. M. Indium phosphide nanowires as

building blocks for nanoscale electronic and optoelectronic devices. *Nature* **2001**, *409*, 66–69.

(20) Gudiksen, M. S.; Lauhon, L. J.; Wang, J.; Smith, D. C.; Lieber, C. M. Growth of nanowire superlattice structures for nanoscale photonics and electronics. *Nature* **2002**, *415*, 617–620.

(21) Thelander, C.; Agarwal, P.; Brongersma, S.; Eymery, J.; Feiner, L.; Forchel, A.; Scheffler, M.; Riess, W.; Ohlsson, B.; Gösele, U.; Samuelson, L. Nanowire-based one-dimensional electronics. *Mater. Today* **2006**, *9*, 28 – 35.

(22) Motohisa, J.; Kohashi, Y.; Maeda, S. Far-field emission patterns of nanowire light-emitting diodes. *Nano Lett.* **2014**, *14*, 3653–60.

(23) Grzela, G.; Paniagua-Domínguez, R.; Barten, T.; Fontana, Y.; Sánchez-Gil, J. A.; Gómez Rivas, J. Nanowire antenna emission. *Nano Lett.* **2012**, *12*, 5481–5486.

(24) van Dam, D.; Abujetas, D. R.; Paniagua-Domínguez, R.; Sánchez-Gil, J. A.; Bakkers, E. P. A. M.; Haverkort, J. E. M.; Gómez Rivas, J. Directional and Polarized Emission from Nanowire Arrays. *Nano Lett.* **2015**, *15*, 4557–4563.

(25) Maslov, A. V.; Ning, C. Z. Far-field emission of a semiconductor nanowire laser. *Opt. Lett.* **2004**, *29*, 572–574.

(26) Maslov, A. V.; Bakunov, M. I.; Ning, C. Z. Distribution of optical emission between guided modes and free space in a semiconductor nanowire. *J. Appl. Phys.* **2006**, *99*, 024314.

(27) Cao, L.; S., W. J.; Park, J.; Schuller, J. A.; Clemens, B. M.; Brongersma, M. L. Engineering light absorption in semiconductor nanowire devices. *Nat. Mater.* **2009**, *8*, 643–647.

(28) Paniagua-Domínguez, R.; Grzela, G.; Gómez Rivas, J.; Sánchez-Gil, J. Enhanced and directional emission of semiconductor nanowires tailored through leaky/guided modes. *Nanoscale* **2013**, *5*, 10582–10590.

(29) Claudon, J.; Gregersen, N.; Lalanne, P.; Gérard, J.-M. Harnessing light with photonic nanowires: fundamentals and applications to quantum optics. *ChemPhysChem* **2013**, *14*, 2393–2402.

(30) Abujetas, D. R.; Paniagua-Domínguez, R.; Sánchez-Gil, J. A. Unraveling the Janus Role of Mie Resonances and Leaky/Guided Modes in Semiconductor Nanowire Absorption for Enhanced Light Harvesting. *ACS Photonics* **2015**, *2*, 921–929.

(31) Traviss, D. J.; Schmidt, M. K.; Aizpurua, J.; Muskens, O. L. Antenna resonances in low aspect ratio semiconductor nanowires. *Opt. Express* **2015**, *23*, 22771–22787.

(32) García de Abajo, F. J. Optical excitations in electron microscopy. *Rev. Mod. Phys.* **2010**, *82*, 209–275.

(33) Adamo, G.; Ou, J. Y.; So, J. S.; Jenkins, S. D.; De Angelis, F.; MacDonald, K. F.; Di Fabrizio, E.; Ruostekoski, J.; Zheludev, N. I. Electron-Beam-Driven Collective-Mode Metamaterial Light Source. *Phys. Rev. Lett.* **2012**, *109*, 217401.

(34) Sapienza, R.; Coenen, T.; Renger, J.; Kuttge, M.; van Hulst, N. F.; Polman, A. Deep-subwavelength imaging of the modal dispersion of light. *Nat. Mater.* **2012**, *11*, 781–787.

(35) Bashevoy, M. V.; Jonsson, F.; MacDonald, K. F.; Chen, Y.; Zheludev, N. I. Hyperspectral imaging of plasmonic nanostructures with nanoscale resolution. *Opt. Express* **2007**, *15*, 11313–11320.

(36) Zhu, X. L.; Ma, J. S., Y. Zhang; Xu, X. F., J. Wu; Zhang, Y.; Han, X. B.; Fu, Q.; Liao, Z. M.; Chen, L.; Yu, D. P. Confined three-dimensional plasmon modes inside a

ring-shaped nanocavity on a silver film Imaged by cathodoluminescence microscopy. *Phys. Rev. Lett.* **2010**, *105*, 127402.

(37) Takeuchi, K.; Yamamoto, N. Visualization of surface plasmon polariton waves in two-dimensional plasmonic crystal by cathodoluminescence. *Opt. Express* **2011**, *19*, 12365–12374.

(38) Coenen, T.; van de Groep, J.; Polman, A. Resonant Modes of Single Silicon Nanocavities Excited by Electron Irradiation. *ACS Nano* **2013**, *7*, 1689–1698.

(39) Yacobi, B. G.; Holt, D. B. *Cathodoluminescence microscopy of inorganic solids*; Springer Science & Business Media, 1990.

(40) Edwards, P. R.; Martin, R. W. Cathodoluminescence nano-characterization of semiconductors. *Semicond. Sci. Technol.* **2011**, *26*, 064005.

(41) Thonke, K.; Tischer, I.; Hocker, M.; Schirra, M.; Fujan, K.; Wiedenmann, M.; Schneider, R.; Frey, M.; Feneberg, M. Nanoscale characterisation of semiconductors by cathodoluminescence. *IOP Conf. Ser.: Mater. Sci. Eng.* **2014**, *55*, 012018.

(42) Spirkoska, D. et al. Structural and optical properties of high quality zinc-blende/wurtzite GaAs nanowire heterostructures. *Phys. Rev. B* **2009**, *80*, 245325.

(43) Osorio, C. I.; Coenen, T.; Brenny, B. J. M.; Polman, A.; Koenderink, A. F. Angle-resolved cathodoluminescence imaging polarimetry. *ArXiv* **2015**, arXiv:1510.07976 [physics.optics].

(44) Brenny, B. J. M.; van Dam, D.; Osorio, C. I.; Gómez Rivas, J.; Polman, A. Azimuthally polarized cathodoluminescence from InP nanowires. *Appl. Phys. Lett.* **2015**, *107*.

(45) Russo-Averchi, E.; Heiss, M.; Michelet, L.; Krogstrup, P.; Nygard, J.; Magen, C.; Morante, J. R.; Uccelli, E.; Arbiol, J.; Fontcuberta i Morral, A. Suppression of three

dimensional twinning for a 100% yield of vertical GaAs nanowires on silicon. *Nanoscale* **2012**, *4*, 1486–1490.

(46) Matteini, F.; Tütüncüoglu, G.; Potts, H.; Jabeen, F.; Fontcuberta i Morral, A. Wetting of Ga on SiOx and its impact on GaAs nanowire growth on silicon. *Cryst. Growth. Des.* **2015**, *15*, 3105–3109.

(47) Coenen, T.; Vesseur, E. J. R.; Polman, A.; Koenderink, A. F. Directional emission from plasmonic Yagi Uda antennas probed by angle-resolved cathodoluminescence spectroscopy. *Nano Lett.* **2011**, *11*, 3779–3784.

(48) Coenen, T.; Vesseur, E. J. R.; Polman, A. Angle-resolved cathodoluminescence spectroscopy. *Appl. Phys. Lett.* **2011**, *99*, 143103.

(49) Born, M.; Wolf, E. *Principles of Optics: Electromagnetic Theory of Propagation, Interference and Diffraction of Light, 7^{th} edition*; Cambridge University Press, 1997.

(50) Stratton, J. A. *Electromagnetic theory*; Read Books, 1941.

(51) Haegel, N. M.; Mills, T. J.; Talmadge, M.; Scandrett, C.; Frenzen, C. L.; Yoon, H.; Fetzer, C. M.; King, R. R. Direct imaging of anisotropic minority-carrier diffusion in ordered GaInP. *J. Appl. Phys.* **2009**, *105*, 023711.

(52) Demers, H.; Poirier-Demers, N.; Couture, A. R.; Joly, D.; Guilmain, M.; de Jonge, N.; Drouin, D. Three-dimensional electron microscopy simulation with the CASINO Monte Carlo software. *Scanning* **2011**, *33*, 135–146.

(53) Palik, E. D. *Handbook of optical constants of solids*; Academic press, 1998; Vol. 3.

(54) Hagemann, H.-J.; Gudat, W.; Kunz, C. Optical constants from the far infrared to the x-ray region: Mg, Al, Cu, Ag, Au, Bi, C, and Al_2O_3. *JOSA* **1975**, *65*, 742–744.

Graphical TOC Entry